Electronic Research Archive

http://www.aimspress.com/journal/era

ERA, 33(12): 7584-7599.
DOI: 10.3934/era.2025335
Received: 10 November 2025
Revised: 08 December 2025
Accepted: 10 December 2025
Published: 18 December 2025

Research article

Stabilized leapfrog scheme preserving the maximum bound principle for the generalized Allen–Cahn equation

Chunjuan Hou[1] **and Baitong Ma**[2,*]

[1] Institute of Artificial Intelligence, Guangzhou Huashang College, Guangzhou 511300, China
[2] School of Mathematics and Statistics, Beihua University, Jilin 132013, China

* **Correspondence:** Email: 1837498081@qq.com.

Abstract: This paper addresses the numerical method for the generalized Allen–Cahn equation featuring nonlinear mobility and a convection term. We propose a linear second–order finite difference scheme that adheres to the discrete maximum bound principle (MBP). The scheme is discretized using the leapfrog finite difference approach, incorporating a stabilized term in time, an upwind scheme for the convection term, and a central–difference scheme for the diffusion term. It is demonstrated that the discrete MBP holds under reasonable constraints on both the time step size and the coefficient of the stabilized term. Additionally, we provide an L^∞–error estimate for our proposed scheme. Several numerical experiments are conducted to validate our theoretical findings.

Keywords: generalized Allen–Cahn equation; finite difference method; maximum bound principle; error estimates.

1. Introduction

In this paper, we investigate the numerical method for the generalized Allen–Cahn equation

$$\begin{aligned} &\frac{\partial \phi}{\partial t} + \boldsymbol{v}\cdot\nabla\phi = M(\phi)\left(\varepsilon\Delta\phi - \frac{1}{\varepsilon}F'(\phi)\right), \quad \boldsymbol{x}\in\Omega,\ t\in(0,T], \\ &\phi(\boldsymbol{x},0) = \phi_0(\boldsymbol{x}), \quad \boldsymbol{x}\in\Omega, \end{aligned} \tag{1.1}$$

subject to appropriate boundary conditions, including periodic boundary conditions, homogeneous Dirichlet boundary conditions, and homogeneous Neumann boundary conditions. Here, Ω represents a bounded domain in R^d $(d = 1, 2, 3)$ with C^1–smooth boundary $\partial\Omega$. The diffuse interface width parameter is positive, and $T > 0$ denotes the terminal time. The function $M(\phi)$ is a nonnegative mobility functional, while $F(\phi) = \frac{1}{4}(\phi^2 - 1)^2$ serves as a double–well potential. Additionally, $\boldsymbol{v}(x,t)$ signifies a given velocity field.

Recently, the Allen–Cahn equation has been extensively employed to model various phenomena such as mean curvature flow [1,2], image segmentation [3], crystalline solids [4], and numerous issues within materials science. Notably, it has emerged as a fundamental model equation for the diffuse interface approach developed to examine phase transitions and interfacial dynamics in materials science; see references [5,6]. In these contexts, an involved velocity field plays a crucial role in the Allen–Cahn phase equation. This aspect serves as one of our motivations for studying this generalized model. Another motivation stems from the fact that nonlinear degenerate mobility can more accurately capture the physics of phase separation since pure phases must exhibit vanishing mobility (see [7,8]).

In contrast to the conventional Allen–Cahn equation [4], the generalized Allen–Cahn equation (1.1) exhibits enhanced complexity due to the incorporation of an additional velocity field and nonlinear mobility. Nevertheless, it maintains the maximum bound principle (MBP) akin to its standard counterpart; specifically, if $\|\phi_0\|_{0,\infty} \leq 1$, then $\|\phi(\cdot,t)\|_{0,\infty} \leq 1, \forall t \in (0,T]$.

Given the inherent difficulty in obtaining exact solutions for these phase–field models, numerical methodologies play an important role in their investigation. Over recent decades, substantial research efforts have been devoted to developing numerical techniques that guarantee MBP and other intrinsic properties for both the Allen–Cahn equation and more generalized phase–field models. Notably, Shen and Tang et al. [9, 10] introduced MBP–preserving, energy–stable implicit–explicit schemes for both standard and generalized Allen–Cahn equations. Hou et al. [11] developed a second–order finite difference scheme with dual parameters that ensures MBP preservation and energy stability. Furthermore, Hou and Leng [12] investigated a Crank–Nicolson/Adams–Bashforth finite difference scheme for the standard Allen–Cahn equation, demonstrating its capability to maintain MBP and energy stability. Additionally, Hou et al. [13] proposed a linear stabilized Crank–Nicolson (CN) scheme that preserves MBP and energy stability for the standard Allen–Cahn equation with general mobility.

Zhu et al. [14] conducted a comprehensive investigation into the nonuniform second–order backward differentiation formula (BDF2) applied to the Allen–Cahn model incorporating general potential and variable mobility. Under moderate temporal step constraints and specific time–step ratio conditions, the nonuniform BDF2 scheme has been rigorously demonstrated to satisfy the discrete MBP. The innovative kernel recombination methodology and MBP–preserving iterative approach have made significant contributions to this analytical framework. Ye et al. [15] investigated the generalized Allen–Cahn–type phase–field crystal model with face–centered–cubic ordering structure (PFC–FCC). They implemented the operator splitting method for this model and developed an efficient second–order numerical scheme, employing the Fourier spectral method for spatial discretization and the strong stability preserving Runge–Kutta (SSP–RK) method for temporal discretization. Shen and Zhang [16] utilized a first–order accurate stabilized implicit–explicit time discretization scheme combined with a fourth–order accurate finite difference method to solve a generalized Allen–Cahn equation coupled with passive convection under a given incompressible velocity field. They demonstrated that the discrete MBP holds under appropriate mesh size and time step constraints, and this finding is extendable to the construction of bound–preserving schemes for any passive convection scenario with an incompressible velocity field. Yang [17] investigated the stabilized semi–implicit temporal scheme and the splitting scheme for the Allen–Cahn equation, which emerges from phase transition phenomena in materials science. Tang [18] developed a second–order accurate, energy–stable, and MBP–preserving scheme for the Allen–Cahn equation with a general mobility, utilizing the stabilized exponential scalar auxiliary variable (SESAV) methodology. Hou et al. [19] proposed a linear second–order numerical ap-

proach for the Allen–Cahn equation with general mobility. Their scheme integrates two–step first– and second–order backward differentiation formulas for temporal approximation with central finite difference for spatial discretization, supplemented by two additional stabilization terms. Li et al. [20] demonstrated that the classical fourth–order accurate compact finite difference scheme, when combined with high–order strong stability preserving time discretizations for convection–diffusion problems, satisfies a weak monotonicity property. This property indicates that a straightforward limiter can enforce the bound–preserving property without compromising conservation or high–order accuracy. Ju et al. [21] developed and analyzed novel first– and second–order stabilized exponential–scalar auxiliary variable (SAV) schemes for a class of Allen–Cahn–type equations. These schemes are proven to simultaneously preserve the energy dissipation law and MBP in discrete settings. Furthermore, optimal error estimates for the numerical solutions are rigorously derived for both schemes. Yang et al. [22] implemented a kth-order single–step temporal scheme combined with a lumped mass finite element method in space, utilizing piecewise rth–order polynomials and Gauss–Lobatto quadrature. They introduced a cut–off post–processing technique to eliminate values that violate the MBP at finite element nodal points at each time level, thereby guaranteeing that the numerical solution adheres to the MBP. Zhang et al. [23] developed and analyzed a class of up to fourth–order maximum principle preserving integrators for the Allen–Cahn equation, addressing the critical question of whether high–order temporal integrators can maintain the MBP. Zhang et al. [24] introduced a class of explicit structure–preserving schemes up to third–order precision for solving the modified Allen–Cahn equation, incorporating either a nonlocal Lagrange multiplier or a local–nonlocal Lagrange multiplier. Zhang and Du [25] investigated numerical approximations for Allen–Cahn–type diffuse interface models, with particular emphasis on the models' performance in approaching the sharp interface limit and the efficacy of high–order discretization schemes. They also conducted a comparative analysis of various spatial discretizations of an energy functional within the diffuse interface framework. Nan and Song [26] developed high–order schemes that maintain the MBP. These schemes are derived by integrating scalar variables with explicit strong stability preserving Runge–Kutta methods and are specifically designed for a particular class of gradient flows. Yang et al. [27] proposed and rigorously analyzed an efficient discontinuous Galerkin method for solving the stochastic Allen–Cahn equation with multiplicative noise. The proposed scheme employs the symmetric interior penalty discontinuous Galerkin finite element for spatial discretization and the implicit Euler scheme for temporal discretization.

In addition, some finite element methods have also been applied to solve the phase–field models such as the Allen–Cahn equation, sometimes enriched with suitable basis functions. Xiao et al. [28] proposed two distinct types of unconditionally maximum principle–preserving finite element schemes for both the standard and conservative surface Allen–Cahn equations. To ensure the preservation of the discrete MBP, they employed the surface finite element method for spatial discretization. For the temporal discretization of the standard Allen–Cahn equation, the stabilized semi–implicit and convex splitting schemes were reformulated into lumped mass forms. Li et al. [29] not only designed and analyzed a second–order numerical method for the Allen–Cahn equation (a model that describes the coarsening of the anti–phase domain in binary alloys), but also conducted rigorous numerical validations to confirm its unconditional energy stability. Yang et al. [30] developed fourth–order temporal unconditional structure–preserving schemes for the Allen–Cahn equation and its conservative forms via mass–lumping finite element space discretization, integrating the integrating factor Runge–Kutta method and the stabilization technique. Recently, Nudo [31] proposed two one–parameter families of

quadratic polynomial enrichments aimed at improving the accuracy of the classical Crouzeix–Raviart finite element method. These enrichments are implemented by employing weighted line integrals as enriched linear functionals and quadratic polynomial functions as enrichment basis. Nudo [32] elaborated a general strategy to improve the Crouzeix–Raviart finite element through the integration of quadratic polynomial functions and three additional general degrees of freedom. In pursuit of this aim, he established a characterization result on the enriched degrees of freedom, providing the necessary support for defining a new enriched finite element. Dell'Accio et al. [33] proposed quadratic and cubic polynomial enrichments for the classical Crouzeix–Raviart finite element, with the objective of constructing accurate approximations within the enriched elements. To achieve this, they incorporated three and seven weighted line integrals, respectively, as additional degrees of freedom.

When solving the Allen–Cahn equation using the linear BDF2 scheme [34], two solves are required at each step, whereas the leapfrog format only requires one solve. Additionally, the leapfrog scheme does not introduce new variables, unlike the SESAV scheme [18], which necessitates adding an exponential scalar auxiliary variable. This increases the complexity of mathematical derivations and incurs additional computational and storage costs associated with this variable.

In this study, we develop a stabilized leapfrog scheme specifically tailored for the generalized Allen–Cahn equation. The remainder of this paper is organized as follows. Section 2 presents the fully discrete scheme. Section 3 is devoted to the proof of the discrete MBP. In Section 4, we derive an L^∞–error estimate. Finally, in Section 5, we carry out numerical experiments to validate the theoretical results.

2. The fully discretized scheme

In this section, we present the fully discretized scheme for (1.1). For the sake of simplicity, we only consider the 1D case ($\Omega = (a, b)$) with homogeneous Dirichlet boundary conditions. It should be noted that the proof techniques for two–dimensional and three–dimensional cases with either periodic or homogeneous Neumann boundary conditions follow a similar approach.

The spatial interval (a, b) and temporal interval $(0, T]$ are discretized using a uniform mesh, where the spatial step size is defined as $h = (b - a)/(N + 1)$ and the temporal step size as $\tau = T/L$, with N and L being positive integers. The set of grid points are denoted by $x_i = a + (i - 1)h$ and $t_n = n\tau$ for $1 \le i \le N + 2$ and $0 \le n \le L$. For notational convenience, we define $\Phi^n = \Phi(x, t_n)$ and $\Phi_i^n = \Phi(x_i, t_n)$.

To solve Eq (1.1), we employ the following leapfrog scheme with a stabilization term, which can be expressed as

$$\frac{\phi^{n+1} - \phi^{n-1}}{2\tau} - \Lambda_1^n A_v^n \phi^n + \beta(\phi^{n+1} + \phi^{n-1} - 2\phi^n) = \Lambda_M^n \left(\varepsilon \frac{D_h(\phi^{n+1} + \phi^{n-1})}{2} - \frac{1}{\varepsilon} F'(\phi^n) \right), \tag{2.1}$$

where $n \ge 1, \beta > 0$, ϕ^n represents the vector of numerical solution at nth level.

For the first step, we use the following second–order CN scheme:

$$\frac{\phi^1 - \phi^0}{\tau} - \Lambda_1^{\frac{1}{2}} \Lambda_v^{\frac{1}{2}} \phi^{\frac{1}{2}} = \Lambda_M^{\frac{1}{2}} \left(\varepsilon \Delta_h \phi^{\frac{1}{2}} - \frac{1}{\varepsilon} F'(\hat{\phi}^{\frac{1}{2}}) \right) - k(\phi^{\frac{1}{2}} - \hat{\phi}^{\frac{1}{2}}), \tag{2.2}$$

where $\hat{\phi}^{\frac{1}{2}}$ is obtained via the following first–order stabilized semi–implicit scheme:

$$\frac{\hat{\phi}^{\frac{1}{2}}-\phi^0}{\tau/2}-\Lambda_1^{\frac{1}{2}}A_v^{\frac{1}{2}}\hat{\phi}^{\frac{1}{2}}=\Lambda_M^0\left(\varepsilon\Delta_h\hat{\phi}^{\frac{1}{2}}-\frac{1}{\varepsilon}F'(\phi^0)\right)-k(\hat{\phi}^{\frac{1}{2}}-\phi^0). \tag{2.3}$$

The differential matrix D_h is given by

$$D_h:=\frac{1}{h^2}\begin{pmatrix}-2 & 1 & & & \\ 1 & -2 & 1 & & \\ & \ddots & \ddots & \ddots & \\ & & 1 & -2 & 1 \\ & & & 1 & -2\end{pmatrix}_{N\times N},$$

the convection term is discretized by upwind scheme, which is expressed as

$$\Lambda_1^{n+1}=\mathrm{diag}(\mathrm{abs}(V^{n+1})),\ V^{n+1}=(v_1^{n+1},v_2^{n+1},\ldots,v_N^{n+1})^T,$$

$$A_v^{n+1}=\frac{1}{2h}\begin{bmatrix}-2 & 1-\mathrm{sgn}\left(v_1^{n+1}\right) & & & & \\ 1+\mathrm{sgn}\left(v_2^{n+1}\right) & -2 & 1-\mathrm{sgn}\left(v_2^{n+1}\right) & & & \\ & \ddots & \ddots & \ddots & & \\ & & 1+\mathrm{sgn}\left(v_{N-1}^{n+1}\right) & -2 & 1-\mathrm{sgn}\left(v_{N-1}^{n+1}\right) & \\ & & & 1+\mathrm{sgn}\left(v_N^{n+1}\right) & -2 & \end{bmatrix}_{N\times N},$$

and $\Lambda_M^n=\mathrm{diag}(M(\phi^n))$, where $M(\phi^n)=\left(M(\phi_1^n),\ldots,M(\phi_N^n)\right)^T$.

3. The discrete maximum principle

In this section, we will demonstrate that the scheme (2.1) preserves the discrete MBP. This preservation result is established based on the following three lemmas, each of which plays a crucial role in laying the necessary theoretical groundwork for our subsequent proof.

Lemma 3.1. *([34]) Let $\phi^0=(\phi_0(x_1),\phi_0(x_2),\ldots,\phi_0(x_N))^T$. Assume that the initial data satisfies $\|\phi_0\|_{0,\infty}\le 1$. Then the scheme* (2.2) *preserves the discrete MBP provided that*

$$k\ge\frac{1}{\varepsilon}\max_{x\in[-1,1]}\left(M'(x)F'(x)+M(x)F''(x)\right), \tag{3.1}$$

$$\frac{2}{\tau}\ge k+\frac{2\varepsilon^2}{h^2}\|M\|_{C[-1,1]}+\frac{1}{h}\|v\|_{C(0,T;C[a,b])}. \tag{3.2}$$

Definition 3.1. Let $A=(a_{ij})\in\mathbb{R}^{n\times n}$ be an n–order real square matrix. A is called a negative diagonally dominant (NDD) matrix if it satisfies the following two core conditions:

1) All diagonal entries are negative, i.e., for any $i\in\{1,2,\ldots,n\}$, $a_{ii}<0$;

2) The absolute value of each diagonal entry is greater than or equal to the sum of the absolute values of all other non–diagonal entries in the same row (row–wise diagonal dominance), i.e., for any $i \in \{1, 2, \ldots, n\}$, the inequality

$$|a_{ii}| \geq \sum_{\substack{j=1 \\ j \neq i}}^{n} |a_{ij}|$$

holds.

Lemma 3.2. *([10]) Let $B = (b_{ij}) \in \mathbb{R}^{N\times N}$ and $A = aI - B$, where $a > 0$. Suppose that B is an NDD matrix. Then we have*

$$\|A^{-1}\|_\infty \leq \frac{1}{a}.$$

Lemma 3.3. *([34]) Denote*

$$g(x) = \beta x - \frac{1}{\varepsilon} M(x)F'(x),\ x \in [-1, 1].$$

Then, we have

$$|g(x)| \leq \beta$$

under the condition

$$\beta \geq \frac{1}{\varepsilon} \max_{x\in[-1,1]} \left(M'(x)F'(x) + M(x)F''(x)\right). \tag{3.3}$$

Theorem 3.1. *Assume that the initial value satisfies* $\max_{x\in[a,b]} |\phi_0(x)| \leq 1$. *Then the fully discrete scheme* (2.1) *preserves the discrete MBP provided that*

$$\beta \geq \max\left\{\frac{1}{h}\|v\|_{C(0,T;C[a,b])}, \frac{1}{\varepsilon} \max_{x\in[-1,1]} \left(M'(x)F'(x) + M(x)F''(x)\right)\right\}, \tag{3.4}$$

$$\tau \leq \frac{1}{2\left(\beta + \frac{\varepsilon}{h^2}\|M\|_{C[-1,1]}\right)}. \tag{3.5}$$

Proof. First, it is evident that $\|\phi^0\|_\infty \leq 1$. Meanwhile, according to Lemma (3.1), we have $\|\phi^1\|_\infty \leq 1$ if k satisfies condition (3.1) and τ satisfies condition (3.2). Then we employ mathematical induction to establish the proof of this theorem. Assume that $\|\phi^{n-1}\|_\infty \leq 1$ and $\|\phi^n\|_\infty \leq 1$ for some n. By rearranging (2.1) and taking L^∞ norm, we have

$$\|\phi^{n+1}\|_\infty \leq \left\|G^{-1}\right\|_\infty \|2\beta\tau\phi^n - \frac{2}{\varepsilon}\tau\Lambda_M^n F'(\phi^n) + (2\beta\tau I + 2\tau\Lambda_1^n A_v^n)\phi^n + ((1 - 2\beta\tau) + \tau\varepsilon\Lambda_M^n D_h)\phi^{n-1}\|_\infty,$$

where $G = (1 + 2\beta\tau)I - \tau\varepsilon\Lambda_M^n D_h$.

Given that A_v^n and D_h are NDD matrices, combined with the nonnegativity of Λ_1^n and Λ_M^n, and considering the property that the product of a nonnegative diagonal matrix and an NDD matrix remains NDD, it can be directly verified that both $\Lambda_1^n A_v^n$ and $\Lambda_M^n D_h$ are NDD matrices.

Observe that each element of $\beta\phi^n - \frac{1}{\varepsilon}\Lambda_M^n F'(\phi^n)$ is of the form $g(x) = \beta x - \frac{1}{\varepsilon}M(x)F'(x)$. It follows from Lemma (3.3) and $\|\phi^n\|_\infty \leq 1$ that we obtain

$$\left\|2\beta\tau\phi^n - \frac{2}{\varepsilon}\tau\Lambda_M^n F'(\phi^n)\right\|_\infty \leq 2\beta\tau\,\|\phi^n\|_\infty \leq 2\beta\tau. \tag{3.6}$$

Applying Lemma (3.2), we get

$$\left\|G^{-1}\right\|_{\infty} \leq (1 + 2\beta\tau)^{-1}. \tag{3.7}$$

Since $\Lambda_M^n D_h$ is an NDD matrix and τ satisfies condition (3.5), we conclude that

$$\|(1 - 2\beta\tau)\phi^{n-1} + \tau\varepsilon\Lambda_M^n D_h\phi^{n-1}\|_{\infty} \leq 1 - 2\beta\tau. \tag{3.8}$$

And as $\Lambda_1^n A_v^n$ is NDD and β satisfies condition (3.4), we have

$$\|(2\beta\tau I + 2\tau\Lambda_1^n A_v^n)\phi^n\|_{\infty} \leq 2\beta\tau. \tag{3.9}$$

Combining the arguments presented in (3.6)–(3.9), we finish the proof.

Remark 3.1. The core origin of conditions (3.2), (3.4), and (3.5) lies in the properties of NDD matrices: By constraining the relationships between parameters k, β and steps τ, h, we ensure that the coefficient matrix corresponding to the discrete scheme satisfies the NDD property, thus providing matrix-level guarantees for preserving the MBP. Conditions (3.1) and (3.3) stem from the need to control the nonlinear source term. By limiting the values of time step k and β, we prevent the nonlinear potential term from causing the numerical solution to exceed the range $[-1, 1]$ during discrete iterations.

Remark 3.2. It should be noted that conditions (3.1)–(3.5) are purely sufficient conditions for MBP preservation, rather than necessary ones. In practice, the MBP may still hold for parameter combinations slightly outside these bounds.

4. Error analysis

In this section, we shall derive the maximum–norm error estimate for the numerical solution generated by the leapfrog scheme (2.1), with the derivation proceeding rigorously based on the discrete MBP preservation result established in Theorem 3.1. Assume $\phi(t_n)$ is the exact solution vector of (1.1) at the grid points. Then $\phi(t_n)$ satisfies

$$\begin{aligned}
&\frac{\phi(t_{n+1}) - \phi(t_{n-1})}{2\tau} - \Lambda_1^n A_v^n \phi(t_n) + \beta(\phi(t_{n+1}) + \phi(t_{n-1}) - 2\phi(t_n)) \\
&= \Lambda_M^n \frac{\varepsilon D_h(\phi(t_{n+1}) + \phi(t_{n-1}))}{2} \\
&\quad + (\Lambda_M(t_n) - \Lambda_M^n)\left(\frac{\varepsilon D_h(\phi(t_{n+1}) + \phi(t_{n-1}))}{2} - \frac{\varepsilon\phi_{xx}^{n+1} + \varepsilon\phi_{xx}^{n-1}}{2}\right) \\
&\quad + (\Lambda_M(t_n) - \Lambda_M^n)\frac{\varepsilon\phi_{xx}^{n+1} + \varepsilon\phi_{xx}^{n-1}}{2} - \frac{1}{\varepsilon}\Lambda_M(t_n)F'(\phi(t_n)) + R^n.
\end{aligned} \tag{4.1}$$

Assume that the exact solution ϕ is sufficiently smooth. Thus, it is easy to get

$$\|R^n\|_{\infty} \leq C(\tau^2 + h). \tag{4.2}$$

Lemma 4.1. *([34]) Assume that the exact solution of* (1.1) *is sufficiently smooth and the initial data* $\|\phi_0\|_{0,\infty} \leq 1$. *Then we have the following error estimate:*

$$\left\|e^1\right\|_{\infty} \leq C(\tau^2 + h).$$

Theorem 4.1. *Assume that the exact solution of* (1.1) *is smooth, and the initial value is smooth and bounded by 1, i.e.,* $\|\phi_0\|_{0,\infty} \le 1$. *If the time step* τ *satisfies condition* (3.5) *and* β *satisfies condition* (3.4)*, the following error estimate holds for the scheme* (2.1)*:*

$$\|\phi^n - \phi(t_n)\|_\infty \le C(\epsilon, \beta, T)(\tau^2 + h).$$

Proof. Denote the error as $e^n = \phi^n - \phi(t_n)$. Subtracting (4.1) from (2.1), we obtain

$$\left[(\frac{1}{2} + \beta\tau)I - \frac{\varepsilon\tau\Lambda_M^n D_h}{2}\right] e^{n+1} = \left[(\frac{1}{2} - \beta\tau)I + \frac{\varepsilon\tau\Lambda_M^n D_h}{2}\right] e^{n-1} + W_1 + W_2 + W_3 + W_4 - \tau R^n, \tag{4.3}$$

where

$$W_1 := \frac{\tau}{\varepsilon}\Lambda_M(t_n)F'(\phi(t_n)) - \frac{\tau}{\varepsilon}\Lambda_M^n F'(\phi^n), \tag{4.4}$$

$$W_2 := \tau(\Lambda_M^n - \Lambda_M(t_n))\left[\frac{\varepsilon D_h(\phi(t_{n+1}) + \phi(t_{n-1}))}{2} - \frac{\varepsilon\phi_{xx}^{n+1} + \varepsilon\phi_{xx}^{n-1}}{2}\right], \tag{4.5}$$

$$W_3 := \tau(\Lambda_M^n - \Lambda_M(t_n))\frac{\varepsilon\phi_{xx}^{n+1} + \varepsilon\phi_{xx}^{n-1}}{2}, \tag{4.6}$$

$$W_4 := \tau(2\beta I + \Lambda_1^n A_v^n)e^n. \tag{4.7}$$

Since $\Lambda_M^n D_h$ and $\Lambda_1^n A_v^n$ are NDD matrices, we have

$$\left\|\left(\left(\frac{1}{2} + \beta\tau\right)I - \frac{\varepsilon\tau\Lambda_M^n D_h}{2}\right)e^{n+1}\right\|_\infty \ge (\frac{1}{2} + \beta\tau)\left\|e^{n+1}\right\|_\infty, \tag{4.8}$$

$$\left\|\left[\left(\frac{1}{2} - \beta\tau\right)I + \frac{\varepsilon\tau\Lambda_M^n D_h}{2}\right]e^{n-1}\right\|_\infty \le (\frac{1}{2} - \beta\tau)\left\|e^{n-1}\right\|_\infty, \quad \tau \le \frac{1}{2\left(\beta + \frac{\varepsilon}{h^2}\|M\|_{C[-1,1]}\right)}, \tag{4.9}$$

$$\|W_4\|_\infty \le 2\beta\tau\|e^n\|_\infty, \quad \beta \ge \frac{1}{h}\|v\|_{C(0,T;C[a,b])}. \tag{4.10}$$

By leveraging the established numerical MBP in conjunction with the existing continuum maximum principle, we can rigorously demonstrate that for any $\boldsymbol{p}, \boldsymbol{q} \in \{\boldsymbol{x} \in \mathbb{R}^N : \|\boldsymbol{x}\|_\infty \le 1\}$

$$\|\Lambda_M(\boldsymbol{p}) - \Lambda_M(\boldsymbol{q})\|_\infty \le L_M\|\boldsymbol{p} - \boldsymbol{q}\|_\infty, \quad \|F'(\boldsymbol{p}) - F'(\boldsymbol{q})\|_\infty \le L_F'\|\boldsymbol{p} - \boldsymbol{q}\|_\infty, \tag{4.11}$$

$$\|\Lambda_M(\boldsymbol{p})\|_\infty \le M, \quad \|F'(\boldsymbol{p})\|_\infty \le M_{F'}, \tag{4.12}$$

where L_M and L_F' are the Lipschitz constants over $[-1, 1]$ and M and $M_{F'}$ represent the bound of Λ_M and F', respectively. It is noted that these constants depend only on the continuous problem, not on (h, τ). By employing Eqs (4.11) and (4.12), we are able to estimate (4.4)–(4.6) as

$$\begin{aligned}\|W_1\|_\infty &\le \frac{\tau}{\varepsilon}\left(\|\Lambda_M(t_n)F'(\phi(t_n)) - \Lambda_M(t_n)F'(\phi^n)\|_\infty + \left\|\Lambda_M(t_n)F'(\phi^n) - \Lambda_M^n F'(\phi^n)\right\|_\infty\right)\\ &\le \frac{\tau}{\varepsilon}\left(ML_F' + M_{F'}L_M\right)\|e^n\|_\infty,\end{aligned} \tag{4.13}$$

$$\|W_2\|_\infty \le C_1\varepsilon\tau h^2 L_M\|e^n\|_\infty, \tag{4.14}$$

$$\|W_3\|_\infty \le C_2\varepsilon\tau L_M\|e^n\|_\infty. \tag{4.15}$$

It follows from (4.8)–(4.15) that

$$(\frac{1}{2}+\beta\tau)\|e^{n+1}\|_\infty \le (\frac{1}{2}-\beta\tau)\|e^{n+1}\|_\infty + \tau\left[2\beta+\frac{1}{\varepsilon}(ML'_F+M_{F'}L_M)+C_3L_M\right]\|e^n\|_\infty + C\tau(\tau^2+h), \tag{4.16}$$

namely,

$$\|e^{n+1}\|_\infty \le (1-\frac{4\beta\tau}{1+2\beta\tau})\|e^{n-1}\|_\infty + \frac{C(\varepsilon,\beta)\tau}{1+2\beta\tau}\|e^n\|_\infty + \frac{C\tau(\tau^2+h)}{1+2\beta\tau}. \tag{4.17}$$

Since $\beta \ge 0$, we have

$$\|e^{n+1}\|_\infty - \|e^{n-1}\|_\infty \le C(\varepsilon,\beta)\tau(\|e^n\|_\infty + \|e^{n-1}\|_\infty) + C\tau(\tau^2+h). \tag{4.18}$$

Summing up (4.18) from 1 to $l-1$ ($2 \le l \le L$), we have

$$\|e^l\|_\infty + \|e^{l-1}\|_\infty \le C(\varepsilon,\beta)\tau\sum_{n=1}^{l-1}(\|e^n\|_\infty + \|e^{n-1}\|_\infty) + C(\epsilon,T)(\tau^2+h^2) + \|e^1\|_\infty + \|e^0\|_\infty. \tag{4.19}$$

Taking into account $\|e^0\|_\infty = 0$ and utilizing Lemma (4.1), we proceed to apply the discrete Grönwall inequality to Eq (4.19), which gives the following estimate:

$$\|e^{n+1}\|_\infty \le C(\epsilon,\beta,T)(\tau^2+h).$$

5. Numerical experiments

In this section, we conduct a series of comprehensive numerical experiments focused on the generalized Allen–Cahn equation given by (1.1), with the primary aim of validating the theoretical results associated with the proposed stabilized leapfrog scheme (2.1). Specifically, these experiments are designed to verify two key aspects of the scheme: first, its ability to preserve the discrete MBP, which is a critical theoretical guarantee for the physical plausibility of numerical solutions; and second, its temporal convergence rates, which reflect the accuracy of the scheme in approximating the exact solution. For the purpose of these numerical tests, the nonlinear mobility term is fixed as $M(\phi) = 1-\phi^2$, a commonly adopted form in studies of Allen–Cahn–type equations that captures relevant nonlinear diffusion behaviors. The experiments will cover a range of parameter settings, initial conditions, and computational grids to ensure the robustness and generality of the validation results.

Example 1. We consider the 1D problem with the initial value

$$\phi_0(x) = 0.3\,\mathrm{rand}(x),\ x \in (0,1),$$

the velocity $\boldsymbol{v}(x,t) = e^t\sin(x)$, and $\varepsilon = 0.04, h = 0.01$. We set $t_{\mathrm{tol}} = 1/160$.

The maximum values of the numerical solutions corresponding to different time step sizes τ are presented in Figures 1–4. The right part of Figure 1 shows that the scheme (2.1) preserves the discrete MBP when $\tau = 0.2t_{tol}, 0.8t_{tol}$, while in the case $\tau = 1.2t_{\mathrm{tol}}$, it violates the discrete MBP.

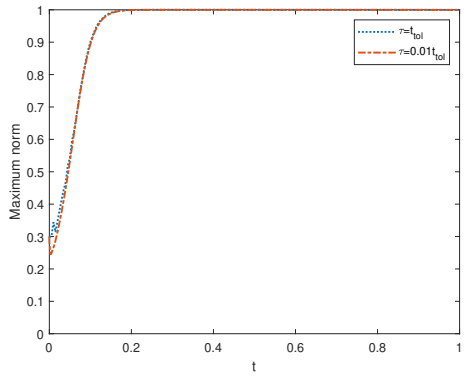

(a) $\tau = t_{\text{tol}}, 0.01t_{\text{tol}}$

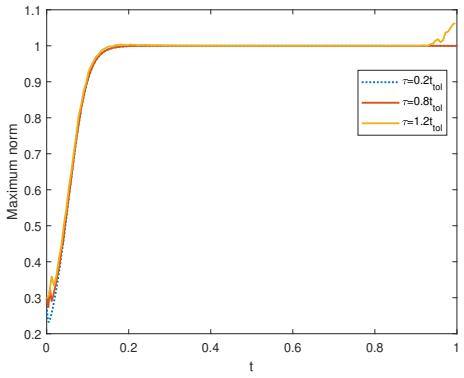

(b) $\tau = 0.2t_{\text{tol}}, 0.8t_{\text{tol}}, 1.2t_{\text{tol}}$

Figure 1. Maximum norms with $\beta = 20$ using different temporal steps.

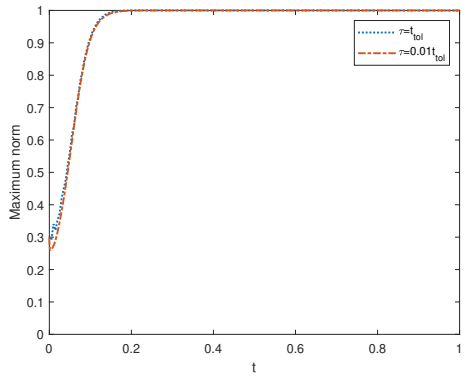

(a) $\tau = t_{\text{tol}}, 0.01t_{\text{tol}}$

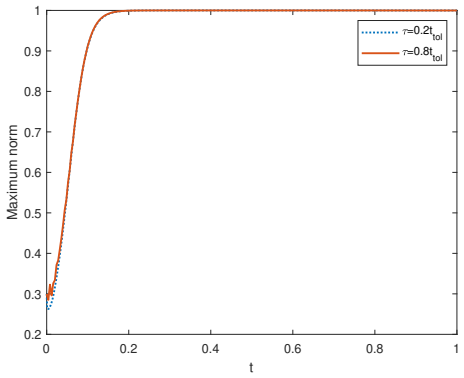

(b) $\tau = 0.2t_{\text{tol}}, 0.8t_{\text{tol}}$

Figure 2. Maximum norms with $\beta = 40$ using different temporal steps.

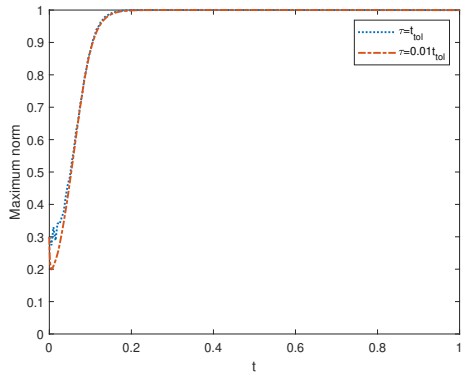

(a) $\tau = t_{\text{tol}}, 0.01t_{\text{tol}}$

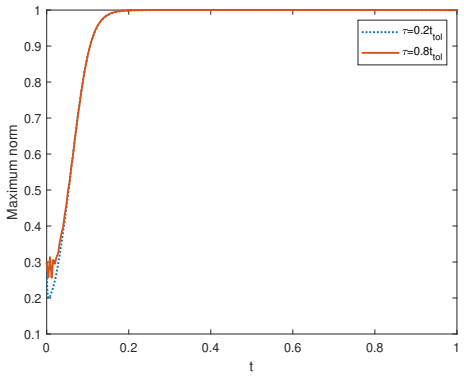

(b) $\tau = 0.2t_{\text{tol}}, 0.8t_{\text{tol}}$

Figure 3. Maximum norms with $\beta = 60$ using different temporal steps.

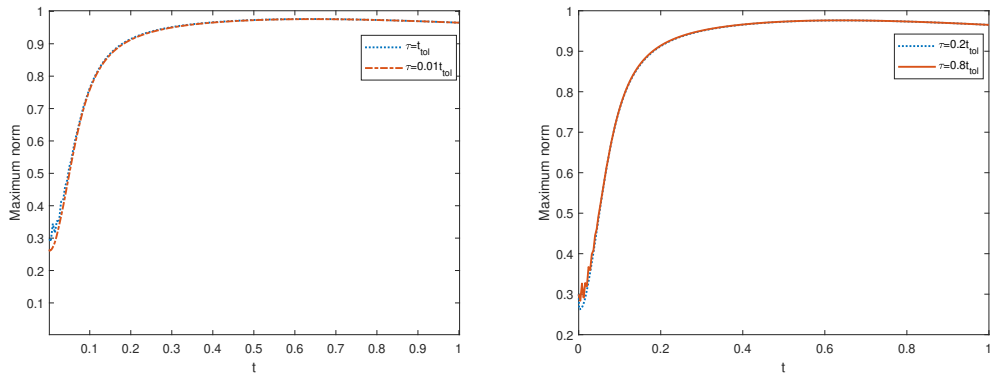

(a) $\tau = t_{\text{tol}}, 0.01t_{\text{tol}}$ **(b)** $\tau = 0.2t_{\text{tol}}, 0.8t_{\text{tol}}$

Figure 4. Maximum norms with $\beta = 80$ using different temporal steps.

Example 2. We consider the 2D Allen–Cahn equation with the initial value

$$\phi_0(x) = 0.9\sin(x)\sin(y),\ (x, y) \in (0, 2\pi)^2,$$

with convection term $\boldsymbol{v}_1(x, y, t) = \pi - x$, $\boldsymbol{v}_2(x, y, t) = y - \pi$, and the parameters are set as $\varepsilon = 0.1$, $k = 4$. To evaluate the temporal convergence rate, we fix the spatial step size as $h = 1/500$ and define the error as $err = \left\|\Phi^{2M} - \Phi^{M}\right\|_{\infty}$. The approximate values of the theoretical error bounds, denoted as C_a, are also listed in Tables 1 and 2. As can be seen from Tables 1 and 2, the obtained convergence order is very close to 2, which verifies the theoretical result presented in Theorem 4.1.

Table 1. Temporal convergence for $\beta = 20, 40$.

	$\beta = 20$			$\beta = 40$		
τ	err	C_a	rate	err	C_a	rate
1/200	2.9204e-04	11.6816	—	9.0504e-04	36.2016	—
1/400	8.0910e-05	12.9456	1.8518	2.5791e-04	41.2656	1.8111
1/800	2.1534e-05	13.7818	1.9097	7.0738e-05	45.2723	1.8663
1/1600	5.5718e-06	14.2638	1.9504	1.8688e-05	47.8413	1.9204
1/3200	1.4193e-06	14.5336	1.9729	4.8159e-06	49.3148	1.9562

Table 2. Temporal convergence for $\beta = 60, 80$.

	$\beta = 60$			$\beta = 80$		
τ	err	C_a	rate	err	C_a	rate
1/200	0.0018	72	—	0.0030	120	—
1/400	5.1772e-04	82.8352	1.8015	8.5192e-04	136.3072	1.8116
1/800	1.4505e-04	92.8320	1.8356	2.4194e-04	154.8416	1.8161
1/1600	3.9019e-05	99.8886	1.8943	6.6080e-05	169.1648	1.8724
1/3200	1.0170e-05	104.1408	1.9398	1.7406e-05	178.2374	1.9246

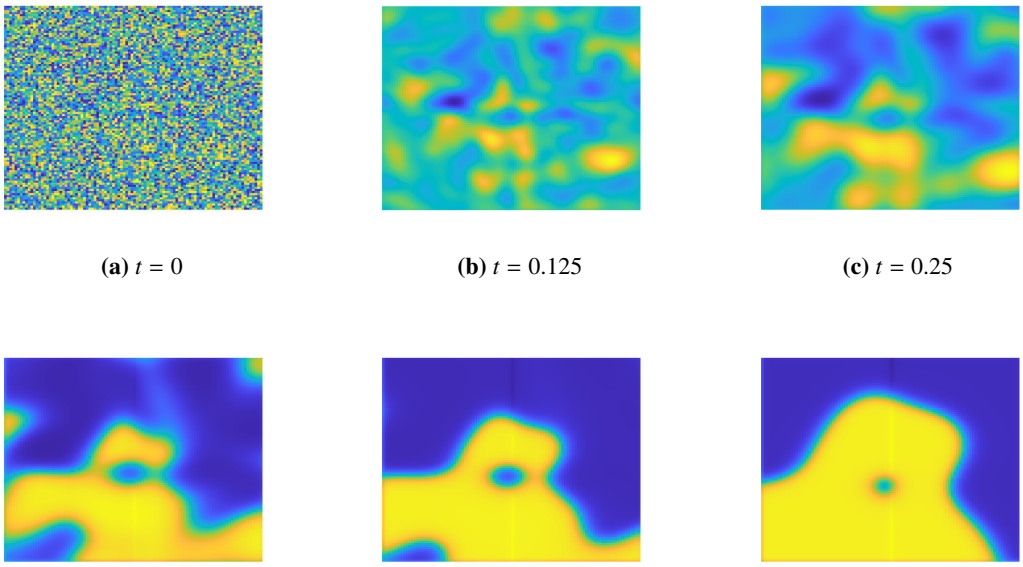

(a) $t = 0$ **(b)** $t = 0.125$ **(c)** $t = 0.25$

(d) $t = 0.375$ **(e)** $t = 0.5$ **(f)** $t = 0.75$

Figure 5. Evolutions of numerical solution for $M(\phi) = 1 - \phi^2$.

Example 3. Consider the 2D Allen–Cahn equation with the following random initial data:

$$\phi_0(x, y) = 0.5\,\mathrm{rand}(x, y) - 0.25,\ (x, y) \in (0, 2\pi)^2.$$

The convection term is defined as $\boldsymbol{v}(x, y, t) = (\pi - x,\ y - \pi)$, and the parameter $\varepsilon = 0.1$. The spatial grid is fixed with $N_x = N_y = 100$. The evolutions of grain coarsening are displayed in Figure 5, where the ordering and coarsening phenomena induced by the convection can be clearly observed.

Table 3. Comparison of time discretization methods for numerical schemes.

Time discretization	MBP conditions	Convergence order
Leapfrog	$\beta \geq \max\left\{\frac{1}{h}\|\|v\|\|_{C(0,T;C[a,b])}, \frac{1}{\varepsilon}\max\limits_{x\in[-1,1]}\left(M'(x)F'(x) + M(x)F''(x)\right)\right\}$, $\tau \leq \frac{1}{2\left(\beta + \frac{\varepsilon}{h^2}\|M\|_{C[-1,1]}\right)}$	$\tau^2 + h$
Linearized CN	$k \geq \frac{1}{\varepsilon}\max\limits_{x\in[-1,1]}\left(M'(x)F'(x) + M(x)F''(x)\right)$, $\frac{2}{\tau} \geq k + \frac{2\varepsilon^2}{h^2}\|M\|_{C[-1,1]} + \frac{1}{h}\|v\|_{C(0,T;C[a,b])}$	$\tau^2 + h$

Example 4. For the generalized Allen–Cahn equation, we consider two linear schemes for comparison, namely the leapfrog scheme and the linearized CN scheme [34]. To begin, a comparison is conducted regarding the conditions for the preservation of the MBP, linearity/nonlinearity, and the convergence

order of the schemes, as presented in Table 3. We consider the 1D problem with the initial value $\phi_0(x) = 0.1\sin(2\pi x)$, $x \in (0, 1)$, and the velocity $\boldsymbol{v}(x, t) = e^t \sin(x)$. For parameter settings, we take $\beta = 40$, $N = 150$, $k = 4$, and $\varepsilon = 0.05$. We then calculate the numerical errors under this set of parameter configurations. It is observed from Table 4 that the proposed scheme in this paper has a shorter CPU time.

Table 4. Temporal convergence with different τ.

	τ	err	Order	CPU time (s)
Leapfrog	1/200	7.0891e-05	—	0.7676
	1/400	1.7840e-05	1.9905	1.4625
	1/800	4.4677e-05	1.9975	3.0412
	1/1600	1.1170e-06	1.9999	5.9659
	1/3200	2.7926e-07	2.0000	11.2308
Linearized CN	1/200	3.0147e-05	—	0.8269
	1/400	8.0756e-06	1.9004	1.5509
	1/800	2.0946e-06	1.9469	3.3442
	1/1600	5.3373e-07	1.9860	6.5729
	1/3200	1.3473e-07	2.0000	11.4581

6. Conclusions

In this study, we investigate numerical approximations for the generalized Allen–Cahn equation, incorporating polynomial potential free energy, nonlinear mobility, and an additional convection term. The stability analysis of the proposed scheme is conducted using a stabilized leapfrog temporal discretization, complemented by central finite difference for the diffusion term and upwind scheme for the advection term in spatial discretization. We establish that the proposed scheme maintains the discrete MBP under appropriate constraints. Numerical experiments are performed to validate the stabilized scheme, and the computational results demonstrate the efficacy of the proposed methodology and corroborating the theoretical findings presented in this work. To conclude, seeking linear temporal schemes with improved order of accuracy that can retain the numerical maximum principle is a worthwhile direction for future studies.

Use of AI tools declaration

The authors declare they have not used Artificial Intelligence (AI) tools in the creation of this article.

Acknowledgments

This work is supported by Guangdong Province Philosophy and Social Science Planning Project (GD24XGL029).

Conflict of interest

The authors declare there are no conflicts of interest.

References

1. X. Feng, A. Prohl, Numerical analysis of the Allen–Cahn equation and approximation for mean curvature flows, *Numer. Math.*, **94** (2003), 33–65. https://doi.org/10.1007/s00211-002-0413-1
2. T. Ilmanen, Convergence of the Allen–Cahn equation to Brakke's motion by mean curvature, *J. Differ. Geom.*, **38** (1993), 417–461. https://doi.org/10.4310/jdg/1214454300
3. M. Beneš, V. Chalupecký, K. Mikula, Geometrical image segmentation by the Allen–Cahn equation, *Appl. Numer. Math.*, **51** (2004), 187–205. https://doi.org/10.1016/j.apnum.2004.05.001
4. S. M. Allen, J. W. Cahn, A microscopic theory for antiphase boundary motion and its application to antiphase domain coarsening, *Acta Metall.*, **27** (1979), 1085–1095. https://doi.org/10.1016/0001-6160(79)90196-2
5. J. Kim, Phase–field models for multi–component fluid flows, *Commun. Comput. Phys.*, **12** (2012), 613–661. https://doi.org/10.4208/cicp.301110.040811a
6. J. Shen, X. Yang, A phase–field model and its numerical approximation for two–phase incompressible flows with different densities and viscosities, *SIAM J. Sci. Comput.*, **32** (2010), 1159–1179. https://doi.org/10.1137/09075860x
7. H. Gomez, T. J. R. Hughes, Provably unconditionally stable, second–order time–accurate, mixed variational methods for phase–field models, *J. Comput. Phys.*, **230** (2011), 5310–5327. https://doi.org/10.1016/j.jcp.2011.03.033
8. Y. Xia, Y. Xu, C. Shu, Local discontinuous Galerkin methods for the Cahn–Hilliard type equations, *J. Comput. Phys.*, **227** (2007), 472–491. https://doi.org/10.1016/j.jcp.2007.08.001
9. J. Shen, T. Tang, J. Yang, On the maximum principle preserving schemes for the generalized Allen–Cahn equation, *Commun. Math. Sci.*, **14** (2016), 1517–1534. https://doi.org/10.4310/cms.2016.v14.n6.a3
10. T. Tang, J. Yang, Implicit–explicit scheme for the Allen–Cahn equation preserves the maximum principle, *J. Comput. Math.*, **34** (2016), 451–461. https://doi.org/10.4208/jcm.1603-m2014-0017
11. T. Hou, D. Xiu, W. Jiang, A new second–order maximum–principle preserving finite difference scheme for Allen–Cahn equations with periodic boundary conditions, *Appl. Math. Lett.*, **104** (2020), 106265. https://doi.org/10.1016/j.aml.2020.106265
12. T. Hou, H. Leng, Numerical analysis of a stabilized Crank–Nicolson/Adams–Bashforth finite difference scheme for Allen–Cahn equations, *Appl. Math. Lett.*, **102** (2020), 106150. https://doi.org/10.1016/j.aml.2019.106150
13. D. Hou, L. Ju, Z. Qiao, A linear doubly stabilized Crank–Nicolson scheme for the Allen–Cahn equation with a general mobility, *Adv. Appl. Math. Mech.*, **16** (2024), 1009–1038. https://doi.org/10.4208/aamm.oa-2023-0067

14. X. Zhu, Y. Gong, Y. Wang, A maximum bound principle–preserving, second–order BDF scheme with variable steps for the generalized Allen–Cahn equation, *Commun. Nonlinear Sci. Numer. Simul.*, **149** (2025), 108897. https://doi.org/10.1016/j.cnsns.2025.108897

15. Y. Ye, X. Feng, L. Qian, A second–order Strang splitting scheme for the generalized Allen–Cahn type phase–field crystal model with FCC ordering structure, *Commun. Nonlinear Sci. Numer. Simul.*, **137** (2024), 108143. https://doi.org/10.1016/j.cnsns.2024.108143

16. J. Shen, X. Zhang, Discrete maximum principle of a high order finite difference scheme for a generalized Allen–Cahn equation, *Commun. Math. Sci.*, **20** (2022), 1409–1436. https://doi.org/10.4310/cms.2022.v20.n5.a9

17. X. Yang, Error analysis of stabilized semi–implicit method of Allen–Cahn equation, *Discrete Contin. Dyn. Syst. - B*, **11** (2009), 1057–1070. https://doi.org/10.3934/dcdsb.2009.11.1057

18. Y. Tang, The stabilized exponential–SAV approach for the Allen–Cahn equation with a general mobility, *Appl. Math. Lett.*, **152** (2024), 109037. https://doi.org/10.1016/j.aml.2024.109037

19. D. Hou, T. Zhang, H. Zhu, A linear second order unconditionally maximum bound principle–preserving scheme for the Allen–Cahn equation with general mobility, *Appl. Numer. Math.*, **207** (2025), 222–243. https://doi.org/10.1016/j.apnum.2024.09.005

20. H. Li, S. Xie, X. Zhang, A high order accurate bound–preserving compact finite difference scheme for scalar convection diffusion equations, *SIAM J. Numer. Anal.*, **56** (2018), 3308–3345. https://doi.org/10.1137/18m1208551

21. L. Ju, X. Li, Z. Qiao, Stabilized exponential–SAV schemes preserving energy dissipation law and maximum bound principle for the Allen–Cahn type equations, *J. Sci. Comput.*, **92** (2022), 1–34. https://doi.org/10.1007/s10915-022-01921-9

22. J. Yang, Z. Yuan, Z. Zhou, Arbitrarily high–order maximum bound preserving schemes with cut–off postprocessing for Allen–Cahn equations, *J. Sci. Comput.*, **90** (2022), 76. https://doi.org/10.1007/s10915-021-01746-y

23. H. Zhang, J. Yan, X. Qian, S. Song, Numerical analysis and applications of explicit high order maximum principle preserving integrating factor Runge–Kutta schemes for Allen–Cahn equation, *Appl. Numer. Math.*, **161** (2020), 372–390. https://doi.org/10.1016/j.apnum.2020.11.022

24. H. Zhang, J. Yan, X. Qian, X. Chen, S. Song, Explicit third–order unconditionally structure–preserving schemes for conservative Allen–Cahn equations, *J. Sci. Comput.*, **90** (2021), 8. https://doi.org/10.1007/s10915-021-01691-w

25. J. Zhang, Q. Du, Numerical studies of discrete approximations to the Allen–Cahn equation in the sharp interface limit, *SIAM J. Sci. Comput.*, **31** (2009), 3042–3063. https://doi.org/10.1137/080738398

26. C. Nan, H. Song, The high–order maximum–principle–preserving integrating factor Runge–Kutta methods for nonlocal Allen–Cahn equation, *J. Comput. Phys.*, **456** (2022), 111028. https://doi.org/10.1016/j.jcp.2022.111028

27. X. Yang, W. Zhao, W. Zhao, Optimal error estimates of a discontinuous Galerkin method for stochastic Allen–Cahn equation driven by multiplicative noise, *Commun. Comput. Phys.*, **36** (2024), 133–159. https://doi.org/10.4208/cicp.oa-2023-0280

28. X. Xiao, R. He, X. Feng, Unconditionally maximum principle preserving finite element schemes for the surface Allen–Cahn type equations, *Numer. Methods Partial Differ. Equ.*, **36** (2020), 418–438. https://doi.org/10.1002/num.22435

29. C. Li, Y. Huang, N. Yi, An unconditionally energy stable second order finite element method for solving the Allen–Cahn equation, *J. Comput. Appl. Math.*, **353** (2018), 38–48. https://doi.org/10.1016/j.cam.2018.12.024

30. J. Yang, N. Yi, H. Zhang, High–order, unconditionally maximum–principle preserving finite element method for the Allen–Cahn equation, *Appl. Numer. Math.*, **188** (2023), 42–61. https://doi.org/10.1016/j.apnum.2023.03.002

31. F. Nudo, Two one–parameter families of nonconforming enrichments of the Crouzeix–Raviart finite element, *Appl. Numer. Math.*, **203** (2024), 160–172. https://doi.org/10.1016/j.apnum.2024.05.023

32. F. Nudo, A general quadratic enrichment of the Crouzeix–Raviart finite element, *J. Comput. Appl. Math.*, **451** (2024), 116112. https://doi.org/10.1016/j.cam.2024.116112

33. F. Dell'Accio, A. Guessab, F. Nudo, New quadratic and cubic polynomial enrichments of the Crouzeix–Raviart finite element, *Comput. Math. Appl.*, **170** (2024), 204–212. https://doi.org/10.1016/j.camwa.2024.06.019

34. Z. Du, T. Hou, A linear second–order maximum bound principle preserving finite difference scheme for the generalized Allen–Cahn equation, *Appl. Math. Lett.*, **158** (2024), 109250. https://doi.org/10.1016/J.AML.2024.109250

AIMS Press